

# A PULSATING HEAT PIPE FOR SPACE APPLICATIONS: GROUND AND MICROGRAVITY EXPERIMENTS

D. Mangini<sup>a</sup>, M. Mameli<sup>a,\*</sup>, A. Georgoulas<sup>a</sup>, L. Araneo<sup>c</sup>, S. Filippeschi<sup>b</sup>, M. Marengo<sup>a,d</sup>

<sup>a</sup>Università di Bergamo, Dipartimento di Ingegnerie e Scienze Applicate, Viale Marconi 5, 24044 Dalmine (BG), Italy.

<sup>b</sup>Università di Pisa, DESTEC, Largo Lazzarino 2, 56122 Pisa, Italy.

<sup>c</sup>Politecnico di Milano, Dipartimento di Energia, Via Lambruschini 4A, 20158 Milano, Italy.

<sup>d</sup>School of Computing, Engineering and Mathematics, University of Brighton, Brighton BN2 4GJ, UK.

\*Corresponding author: mauro.mameli@unibg.it

## ABSTRACT

A novel concept of a hybrid Thermosyphon/Pulsating Heat Pipe with a diameter bigger than the capillary limit is tested both on ground and in hyper/micro gravity conditions during the 61<sup>st</sup> ESA Parabolic Flight Campaign. The device is filled with FC-72 and it is made of an aluminum tube (I.D. 3 mm) bent into a planar serpentine with five curves at the evaporator zone, while a transparent section closes the loop, allowing fluid flow visualizations in the condenser zone. Five heaters, mounted alternatively in the branches just above the curves at the evaporator zone, provide an asymmetrical heating thus promoting the fluid flow circulation in a preferential direction. The device has been tested at different positions (vertical and horizontal) and at different heat power input levels (from 10 W to 160 W). Ground tests show that effectively the device works as a thermosyphon when gravity assisted: in vertical position the device can reach an equivalent thermal resistance of 0.1 K/W with heat fluxes up to 17 W/cm<sup>2</sup>. In horizontal position the fluid motion is absent, thus the device works as a pure thermal conductive medium. The parabolic flight tests point out a PHP working mode: during the micro-gravity period, the sudden absence of buoyancy force activates an oscillating slug/plug flow regime, typical of the PHP operation, allowing the device to work also in the horizontal position. In some cases the hyper-gravity period is able to eliminate partial dry-outs restoring the correct operation until the occurrence of the next microgravity period.

**Keywords:** Pulsating Heat Pipe, Microgravity, Flow visualization, Capillary limit, Thermosyphon, asymmetric heating.

## NOMENCLATURE

Variable	Description	Unit
<i>Bo</i>	Bond Number	[-]
<i>d</i>	Diameter	[m]

$FR$	Filling Ratio	[-]
$g$	Gravity Acceleration	[m/s <sup>2</sup> ]
$Ga$	Garimella Number	[-]
$\dot{Q}$	Heat Input Power	[W]
$R$	Thermal Resistance	[K/W]
Re	Reynolds Number	[-]
$T$	Temperature	[°C]
$U$	Fluid Velocity	[m/s]
$We$	Weber Number	[-]
$\mu$	Dynamic Viscosity	[Pa·s]
$\rho$	Density	[kg/m <sup>3</sup> ]
$\sigma$	Surface Tension	[N/m]

31

## 32 SUBSCRIPTS

<b>Variable</b>	<b>Description</b>
$Bo$	Bond Number
$c$	Condenser Zone
cr	critical
$e$	Evaporator Zone
$eq$	Equivalent
$Ga$	Garimella Number
$l$	Liquid Phase
max	Maximum
min	Minimum
Re	Reynolds Number
$v$	Vapor Phase
$We$	Weber Number

## 33 1 INTRODUCTION

34 In the last decades the role of two-phase passive heat transfer devices in space thermal control  
35 systems gained more and more relevancy because of their lightweight, high performances and  
36 reliability. For instance, when heat dissipation rates become very high, heat pipes are preferred to  
37 honeycomb structures in radiators panels and they have been widely used to reduce temperature

38 gradients too. The Capillary Pumped Loops (CPL) and Loop Heat Pipes (LHP) technologies have  
39 been successfully used as thermal control systems in a large number of missions because of their  
40 ability to cover tortuous and longer paths (up to 5 meters against gravity, during ground tests) [1].  
41 The ability to transport heat efficiently over long distances is due to the presence of a capillary, or  
42 “wick” structure, which is also the more complex and expensive element inside the system.  
43 In order to reduce the effectiveness to cost ratio, more than twenty years ago Akachi [2] introduced  
44 an innovative concept of wickless two phase loop, most known as Pulsating Heat Pipe, consisting  
45 simply in a small diameter tube or channel, bended in several turns, with alternated heated and  
46 cooled zones. The pipe is evacuated and partially filled with a working fluid that resides in the form  
47 of liquid slugs and vapor plugs train thanks to the slight predominance, at least in the static  
48 condition, of capillary forces with respect to buoyancy forces. The heated vapor plugs expand and  
49 push the adjacent fluid towards the cold zone where heat is rejected and vapor condenses, recalling  
50 the adjacent fluid back to the evaporator zone. This process results in a chaotic and oscillating fluid  
51 motion as well as flow pattern transitions [3], nevertheless, the system is able to reach a pseudo-  
52 steady state in a wide range of working conditions [4]. The PHP internal diameter is usually less  
53 than the static critical diameter defined as  $d_{cr} = 2\sqrt{\sigma / g(\rho_l - \rho_v)}$  [5]. Despite the fact that, in this  
54 condition, the capillary forces are strong enough to create an initial slug-plug configuration, gravity  
55 and inertia forces still play a crucial role. When the device is gravity assisted (vertical or bottom  
56 heated mode), the flow motion is more vigorous and the thermal performance is higher with respect  
57 to the case when the PHP is perfectly horizontal and gravity acceleration is always normal to the  
58 main flow path direction [6,7]. It is quite complex to build a PHP, which is gravity-independent on  
59 ground, even if some successful attempts of performance independent on orientation have been  
60 proposed with three-dimensional layouts [8,9]. In this regard, microgravity experiments are  
61 mandatory if one is interested to decouple completely the buoyancy from the inertia effects. By the  
62 time being, several experiments in microgravity conditions have been performed: Gu et al. [10]  
63 have been the first testing a transparent tube PHP [11] and a Flat Plate PHP in zero gravity  
64 conditions, concluding that under reduced gravity the PHP showed better heat transport  
65 performance than that under normal and hypergravity. Taking a deep look at their results this  
66 assessment is clear only when the device works in top heated mode (i.e. when the evaporator above  
67 the condenser). Mantelli et al. [12] provided a similar conclusion testing a planar copper tube PHP  
68 (sixteen turns, 1.27mm I.D.), on a suborbital sounding rocket flight. In order to verify the effect of  
69 the gravity field on a perfectly planar PHP both in bottom heated mode and in horizontal position,  
70 Mameli et al. [13] tested the dynamic response to the gravity field of a planar copper tube PHP

71 (sixteen turns, 1.1mm I.D.) filled with FC-72 during the 58<sup>th</sup> ESA Parabolic Flight Campaign,  
 72 showing that the horizontal PHP performance was not affected by the gravity field variation  
 73 occurring during the parabolic trajectories. Furthermore they performed ground tests by tilting the  
 74 device from the vertical to the horizontal position during operation, showing a clear analogy with  
 75 the thermal response of the vertical PHP under the transition from hypergravity to microgravity and  
 76 viceversa. In the bottom heated mode, the PHP never showed a better heat transfer under reduced  
 77 gravity: the evaporator temperatures tend to increase towards the same values obtained during the  
 78 horizontal tests on ground.

79 Both Gu et al. [10] and Mameli et al. [13] illustrated the possibility to build a PHP for space  
 80 application with an internal diameter bigger than the static critical diameter on ground. Under  
 81 reduced gravity, body forces are negligible and the threshold diameter to obtain a slug-plug  
 82 configuration increases. Since the mass of the thermal fluid per unit length is proportional to the  
 83 square of the I.D, increasing the inner diameter is also beneficial in terms of total heat exchanged.  
 84 Theoretically for  $g = 0 \text{ m/s}^2$  the capillary diameter tends to infinite, anyway, the limit to the increase  
 85 of the inner diameter is also given by inertial and viscosity effects, in the sense that when the fluid  
 86 velocity is high, the menisci are unstable and the slug-plug condition is only possible for smaller  
 87 diameters with respect to the capillary limit. The dynamic threshold levels, evaluated by means of  
 88 Weber and Garimella criteria proposed by Mameli et al. [13],  $d_{we} \leq 4\sigma/\rho_l U_l^2$  and

89  $d_{Ga} \leq \sqrt{\frac{160\mu_l}{\rho_l U_l}} \sqrt{\frac{\sigma}{(\rho_l - \rho_v) \cdot g}}$ , may be more suitable to define the limit for space applications, even if

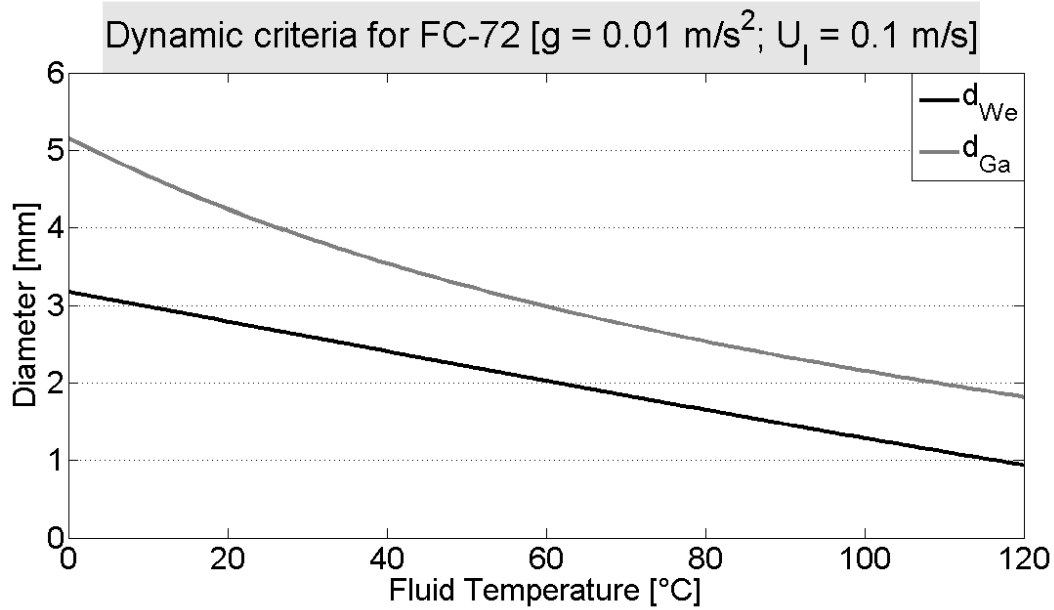
90 further experimental validations are necessary. In order to provide some order of magnitudes, Table  
 91 1 shows the confinement diameters relatively to static and dynamic criteria both in earth and  
 92 microgravity conditions for FC-72 at 20°C, assuming a fluid mean bulk velocity of 0.1 m/s and a  
 93 microgravity level of 0.01m/s<sup>2</sup>, while Figure 1 shows only the dynamic threshold diameters over  
 94 fluid temperature.

95

96 **Table 1: Confinement diameters for FC-72 at 20°C accordingly to static and dynamic criteria.**

FC-72 @ 20°C	$d_{cr}$ [mm] (static)	$d_{Ga}$ [mm] ( $U_l=0.1\text{m/s}$ )	$d_{we}$ [mm] ( $U_l=0.1\text{m/s}$ )
Earth $g=9.81 \text{ m/s}^2$	1.48	0.75	2.79
Microgravity $g=0.01 \text{ m/s}^2$	46.27	4.20	

97



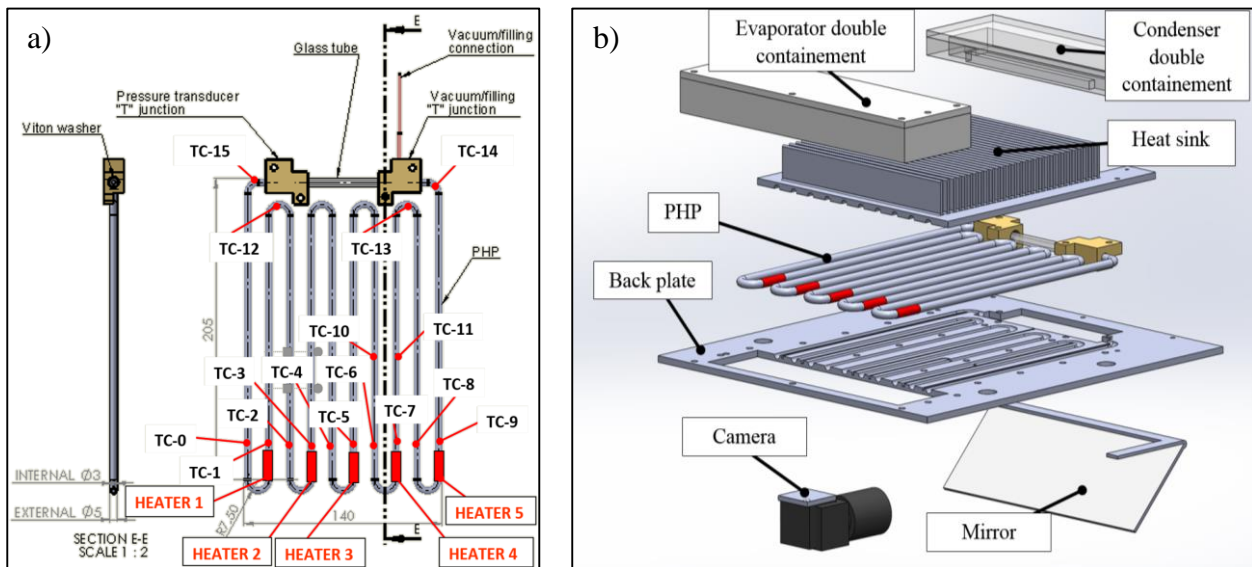
98 **Figure 1: Dynamic threshold diameters for FC-72 for different fluid temperatures evaluated at an**  
 99 **average bulk velocity of the fluid equal to 0.1 m/s and a microgravity level of 0.01 m/s<sup>2</sup>.**

100 The aim of the present work is to prove, also by means of a first flow visualization, that a two-phase  
 101 wickless closed PHP with a diameter bigger than the static critical one on ground can work as a  
 102 PHP (i.e. slug oscillating flow) under the occurrence of microgravity conditions, opening the  
 103 frontiers to a new family of Pulsating Heat Pipes only for space applications.

## 104 2 EXPERIMENTAL APPARATUS AND PROCEDURE

105 Following the discussion above and the diameter thresholds (Table 1), an aluminum Closed Loop  
 106 PHP with 3 mm internal diameter filled with FC-72 have been tested at different heat loads (up to  
 107 160 W), orientations (BHM, horizontal), transient gravity levels (0 g, 1 g, 1.8 g) during the 61<sup>st</sup>  
 108 ESA Parabolic Flight Campaign. The proposed cooling device is made of an aluminum tube  
 109 (I.D./O.D. 3.0 mm/5.0 mm; Total length: 2.55 m) bended into a planar serpentine with ten parallel  
 110 channels and five turns at the evaporator (all curvature radii are 7.5 mm), as shown in Fig. 2a. Two  
 111 “T” junctions allow to close the serpentine in a loop and to derive two ports at each side: one hosts a  
 112 pressure transducer (Kulite<sup>®</sup>, XCQ-093, 1.7 bar A), while the second one is devoted to the vacuum  
 113 and filling procedures. The working fluid is FC-72 and the volumetric filling ratio is 0.5  
 114 corresponding to 8.3 ml. The PHP external tube wall is equipped with sixteen “T” type  
 115 thermocouples (bead diameter 0.2 mm), with an accuracy of  $\pm 0.1$  K after calibration: ten located in  
 116 the evaporator zone and six in the condenser zone, as illustrated in Figure 2a. One additional  
 117 thermocouple is utilized to measure the ambient air temperature. A glass tube fixed between the two

118 “T” junctions, allows the flow pattern visualization in the top of the condenser zone and it also  
 119 closes the loop. The device, the “T” junctions and the glass tube are sealed together, by applying a  
 120 low vapor pressure glue (Varian Torr Seal®).

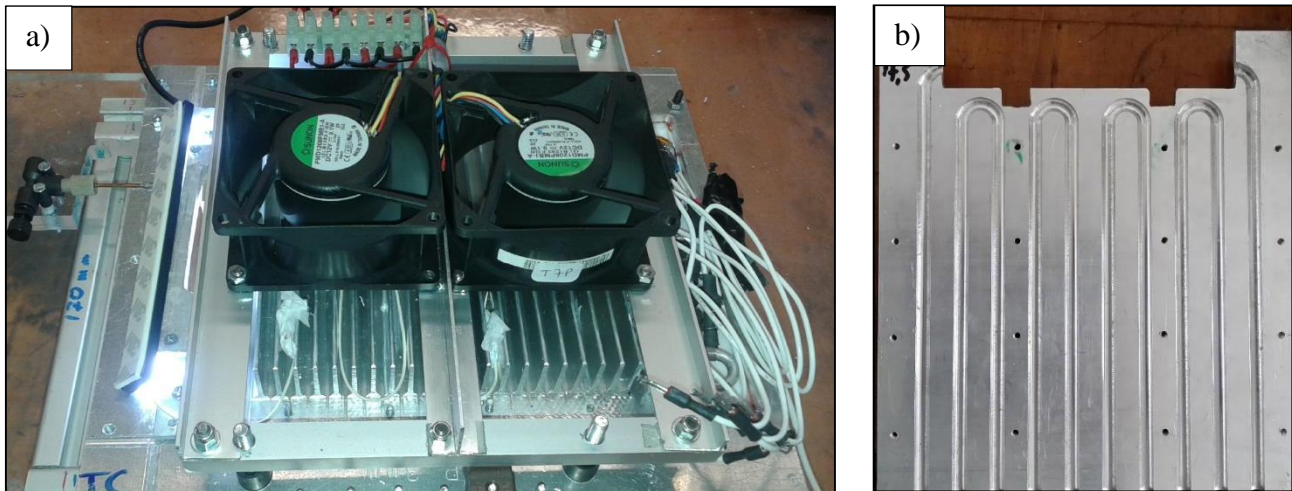


121 **Figure 2: a) thermocouples and heaters location along the PHP tube; b) the test cell with all its**  
 122 **components.**

123 The Figure 2b shows an exploded view of the test cell, highlighting all its main components. In  
 124 order to record the fluid dynamics, a compact camera (Ximea®, MQ013MG-ON objective:  
 125 Cosmimar/Pentax® C2514-M) is positioned behind the PHP by means of an aluminum plate. Due to  
 126 space restrictions, an inclined mirror is also utilized to reach the desired field of view. Diminishing  
 127 the region of interest solely at the glass tube, the camera acquires up to 450 fps, with a resolution of  
 128 1280x200 pixel. The aluminum tube is firstly evacuated by means of an ultra-high vacuum system  
 129 (Varian® DS42 and TV81-T) down to 0.3 mPa and then it is filled up with the working fluid (FC-  
 130 72). The working fluid is firstly degassed within a secondary tank, by continuous boiling and  
 131 vacuuming cycles as described by Henry et al. [14]. The aluminum tube is finally filled with a  
 132 volumetric ratio of  $0.5 \pm 0.03$  and permanently sealed, by means of tin soldering. The difference  
 133 between the actual fluid pressure inside the tube and its saturation pressure, at the ambient  
 134 temperature, gives an indication of the incondensable gas content (less than 6 PPM).

135 The device is equipped with five electrical heaters (Thermocoax® Single core 1Nc Ac, 0.5 mm  
 136 O.D., 50  $\Omega$ /m, each wire is 720 mm long) wrapped just above the evaporator U-turns (Figure 2a)  
 137 covering a tube portion of 20 mm and providing an asymmetric heating on the device. The parallel  
 138 assembly of the heaters is connected with a power supply (GWInstek® 3610A) that can provide an  
 139 electric power input up to 160 W, corresponding to a wall to fluid radial heat flux up to 17 W/cm<sup>2</sup>.

140 Due to the low thermal inertia of the heating system, the pseudo steady state condition can be  
141 reached in approximately 3 minutes. The condenser section is 165 mm long and it is embedded into  
142 a heat sink, which is cooled by means of two air fans (Sunon® PMD1208PMB-A), as shown in  
143 Figure 3a. In order to optimize the thermal contact, circular cross section channels are milled on  
144 both the heat sink and the back plate (Figure 3b).



145 **Figure 3: a) air fan system mounted above the heat sink; b) milled heat sink.**

146 These elements are covered by heat sink compound (RS® Heat Sink Compound) before assembling.  
147 The ambient temperature is kept constant to  $20\text{ °C} \pm 1\text{ °C}$  during the tests. A three-axis g-sensor  
148 (Dimension Engineering®, DE-ACCM3d) is utilized in order to detect the gravity variations during  
149 each parabola. The cooling device, the thermocouples, the pressure transducer, the g-sensor, the  
150 heating and cooling system as well as the visualization system are placed on a beam structure by  
151 means of four anti-vibration bushes. All these components apart from the g-sensor can be orientated  
152 both horizontally and vertically (bottom heat mode).

153 A data acquisition system (NI-cRIO-9073®, NI-9214®, NI-9215®) records the output of the  
154 thermocouples, the pressure transducer and the g-sensor and all signals are recorded at 10 Hz. The  
155 high-speed camera is connected to an ultra-compact PC (NUC® Board D54250WYB) able to store  
156 the images up to 450 fps.

157 The experimental parameters are:

- 158 - The heat input level: from 10 W to 160 W for the bottom heat mode orientation and from 10 W  
159 to 80 W for the horizontal orientation.
- 160 - The gravity field: Normal gravity (1g) during the test on ground and during the straight flight  
161 trajectory; hyper-gravity (1.8g) before and after the parabola during the ascending and

162 descending maneuvers (duration: 20-25 s each); microgravity during the parabola (duration: 20-  
163 21 s).

164 - The orientation: Bottom Heated mode (BHM) and horizontal position.

165 The measured quantities are:

166 - Tube wall temperatures: 10 measuring points in the evaporator zone, 6 in the condenser zone and  
167 1 measuring point that monitors the ambient air temperature.

168 - Local fluid pressure in the condenser zone

169 - Acceleration: the gravity field variation during each parabola is monitored by means of a three-  
170 axis accelerometer.

171 In addition, a video (80 seconds at 450 fps) is recorded during each parabola, starting ten seconds  
172 before the maneuver and stopping around ten seconds after the second hyper-gravity period.

### 173 **3 EXPERIMENTAL RESULTS**

174 In the present section, results are presented in terms of temperature and pressure temporal  
175 evolutions while images of the flow pattern within the condenser zone are also illustrated. The  
176 red/yellow lines indicate the temporal evolution of the temperatures in the evaporator zone just  
177 above the heater (TC1, TC3, TC5, TC7, TC9); the pink color variations correspond to the  
178 temperatures at the evaporator zone far from the heaters (TC0, TC2, TC4, TC6, TC8); the  
179 temperatures recorded in the condenser zone are illustrated with blue color variations (TC10, TC11,  
180 TC12, TC13, TC14, TC15), while the ambient temperature is visible in green. To mention is that  
181 the secondary y-axis at the right corresponds to the heat input levels during the thermal  
182 characterization on ground, and the gravity acceleration in case of flight tests.

183 The overall equivalent thermal resistance is evaluated at each heat input step by the following  
184 equation.

$$R_{eq} = \Delta \bar{T}_{e-c} / \dot{Q} \quad (1)$$

185 Where  $\Delta \bar{T}_{e-c}$  is the difference between the evaporator and the condenser average temperatures in the  
186 pseudo-steady state, and  $\dot{Q}$  is the effective heat power input provided to the evaporator zone.

#### 187 **3.1 Ground tests**

188 The device has been thermally characterized on ground (earth gravity conditions) in vertical (BHM:  
189 bottom heated mode) and in horizontal orientation with heat power input levels up to 160W and 80



190 W respectively, for a duration of 15 minutes in each power input step (see **Errore. L'origine**  
191 **riferimento non è stata trovata.**).

192 **Table 2. Heat power input levels set up for ground tests.**

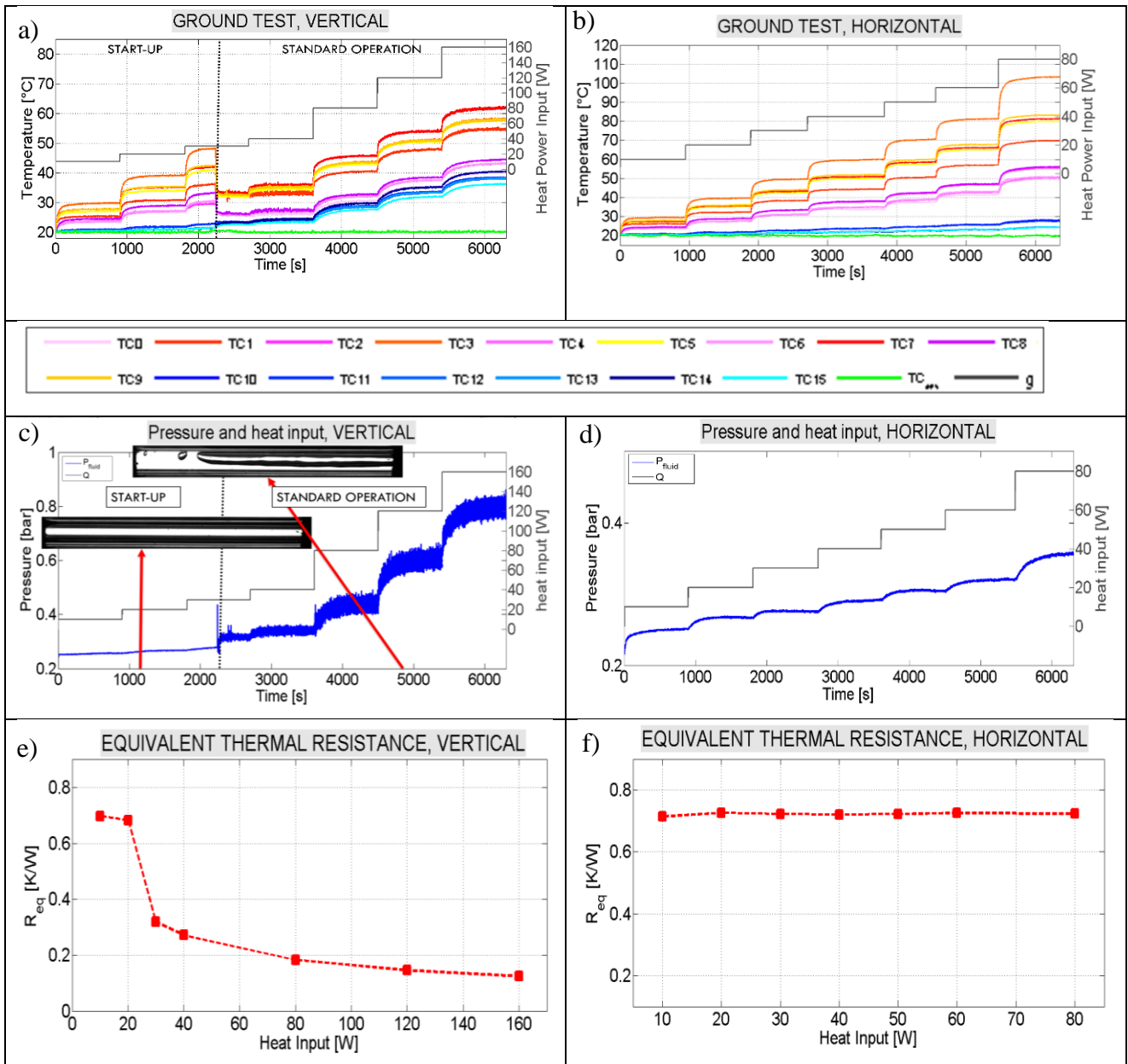
Heat power input levels	
Vertical (Bottom heated)	Horizontal orientation
10 W	10 W
20 W	20 W
30 W	30 W
40 W	40 W
80 W	50 W
120 W	60 W
160 W	80 W

193

194 In the vertical position the device works as a Closed Loop Two Phase Thermosyphon (TS mode)  
195 where the fluid circulation can be obtained from the bubble lift principle defined by Franco et al.  
196 [15] which is explained thoroughly in the next section.

### 197 3.1.1 **Bottom heated mode (BHM)**

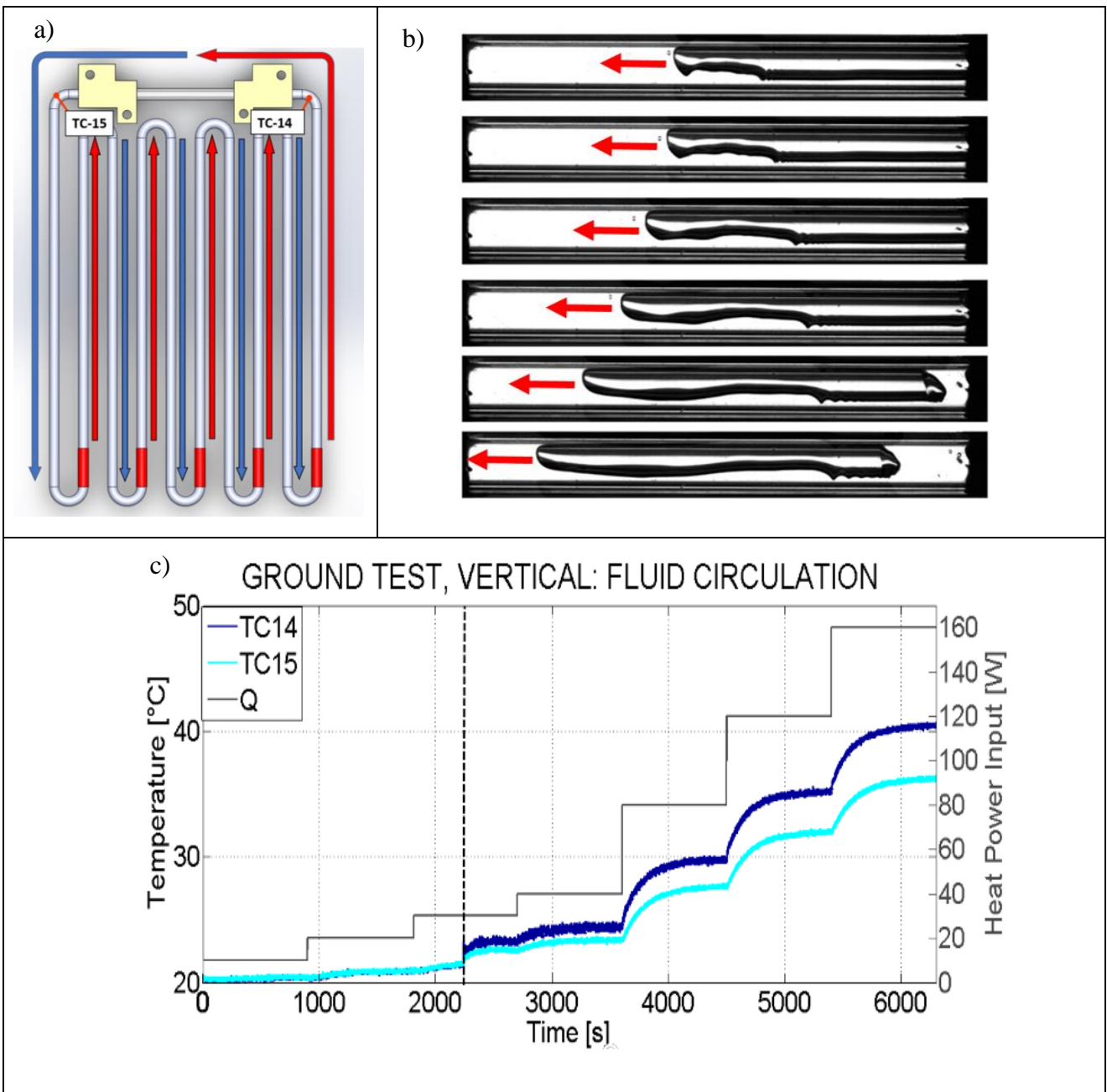
198 In the vertical position, two different working modes can be recognized: (i) the start-up and (ii) the  
199 standard operation [3]. During the start-up, the heat input up to 30W is not sufficient to pump the  
200 fluid batches up to the condenser zone. The liquid phase remains relegated in the evaporator  
201 section, and no fluid motion can be identified in the condenser zone, since the pressure readings do  
202 not exhibit any fluctuations and the transparent tube section appears completely dry (Figure 4c). As  
203 a consequence, the higher the heat power input, the higher the temperatures in the evaporator zone  
204 (Figure 4a), and the equivalent thermal resistance reaches approximately 0.7 K/W (Figure 4e)  
205 during the start-up. When the heat power input is set at 30 W, the higher pressure reached in the  
206 evaporator zone is sufficient to pump the liquid batches in the condenser zone: the pressure signals  
207 shows suddenly vigorous fluctuations and a slug/plug flow is observed in the transparent horizontal  
208 section (Figure 4c). Therefore, the heat exchange is enhanced by convection, the equivalent thermal  
209 resistance decreases, arriving at 0.1 K/W at 160 W of heat power input (Figure 4e), without any  
210 thermal crisis.



211 **Figure 4: Temperature temporal evolutions, pressure temporal evolutions and equivalent thermal**  
 212 **resistance during thermal characterization on ground, first column: vertical operation, second**  
 213 **column: horizontal operation.**

214 Furthermore, the asymmetrical position of the heaters has a direct effect on the fluid motion. In the  
 215 heated branches (up-headers) the fluid batches are lifted up from the evaporator to the condenser in  
 216 the form of non-coherent slugs, by means of the expanding vapor bubbles; along the adjacent  
 217 branches (down-comers) the gravity head assists the return of the fluid from the condenser down to  
 218 the evaporator zone, as shown in Figure 5a. The alternation of up-headers and down-comers  
 219 generates a fluid motion in a preferential direction, activating a net circulation. Temperatures at the  
 220 edges of the transparent section are equal during the start-up, because there is no fluid motion.

221 However, as soon as the fluid starts to reach the condenser zone, TC 14 starts to show higher values  
 222 than TC 15 (Figure 5c). The fluid that is pumped from the up-header, releasing thermal energy  
 223 during its passage through the T-junctions and the transparent section, reaches the other end with a  
 224 lower temperature. This can also be observed through the transparent section of the condenser that  
 225 connects directly the up-header and the down-comer at the right and left sides of the device  
 226 respectively. As it can be observed from the sequence of images recorded at 100 Hz, in Figure 5b,  
 227 the leading edge of the vapor bubble points out a fluid motion from the right to the left, further  
 228 confirming the net circulation in a preferential direction.



229 **Figure 5: Fluid net circulation during the vertical tests: a) fluid direction; b) flow visualization**  
 230 **(100 fps); c) temperatures at the edges of the glass tube.**

231 **3.1.2 Horizontal orientation**

232 When the device is positioned in the horizontal orientation, gravity is never assisting the fluid  
233 motion. Therefore, since the fluid is stratified and the whole vapor phase resides in the upper half of  
234 the tube, its expansion is not able to push the fluid and the device works practically as a purely  
235 conductive medium. The equivalent thermal resistance stabilizes to a constant value of  
236 approximately 0.7 K/W, since the motion of the fluid is not activated for all the heat power inputs  
237 tested. This confirms the importance of having a gravity head between the evaporator and the  
238 condenser zone for TS. Moreover, it was observed that temperatures increase as the heat power  
239 input increases (Figure 4a) and the pressure measured in the condenser zone does not exhibit any  
240 fluctuation (Figure 4b).

241 **3.2 Flight tests**

242 Microgravity experiments have been performed aboard the ESA/Novespace Airbus A300, during  
243 the 61<sup>st</sup> ESA PF campaign. A total of 31 parabolic trajectories are performed in each flight: the first  
244 one, called parabola zero, is followed by six sequences, each consisting of five consecutive  
245 parabolic maneuvers. All sequences are separated by five minute interval at earth g-level. Each  
246 parabolic maneuver is itself subdivided into three parts: 20 s at 1.8 g (hyper-gravity), followed by  
247 22 s at 0.01 g (micro-gravity) and finally 20-25 s at 1.8 g (hyper-gravity). A 90 s period of earth g-  
248 level is in between each parabolic event [16]. One flying day has been devoted to each of the two  
249 experiments summarized in Table 3, PF-I and PF-II respectively. Finally, the third day of the  
250 campaign is devoted to ensure the repeatability of the horizontal test, as will be explained more  
251 thoroughly in section 3.2.2. The heat input level is changed during the five minutes pause at normal  
252 g between each sequence, in order to reach the pseudo-steady state before the beginning of the  
253 parabolic trajectories (1g, 1.8g, 0g, 1.8g, 1g). This procedure is followed in all of the six sequences,  
254 ensuring data repeatability.

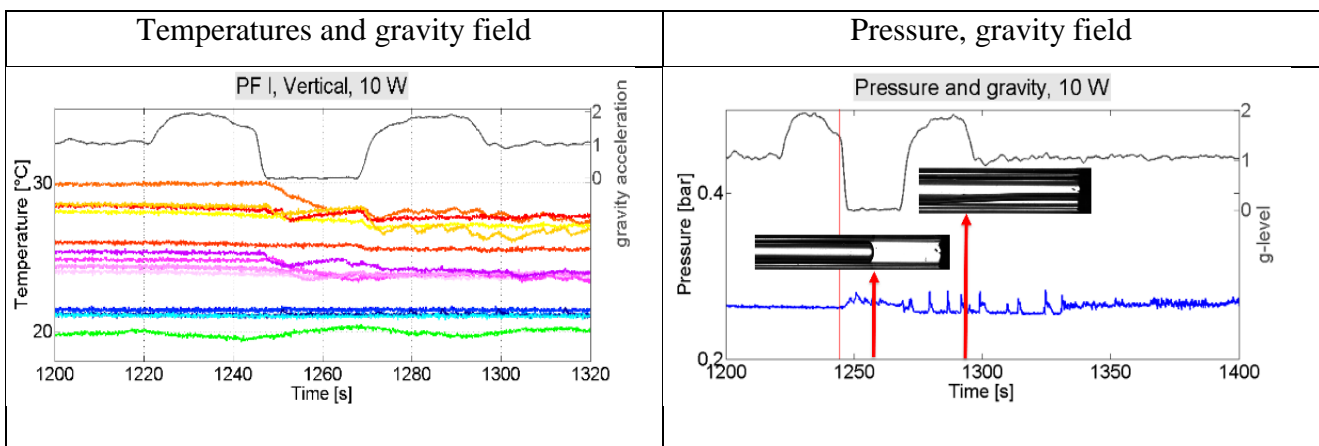
255 **Table 3. Heat power inputs during flight days.**

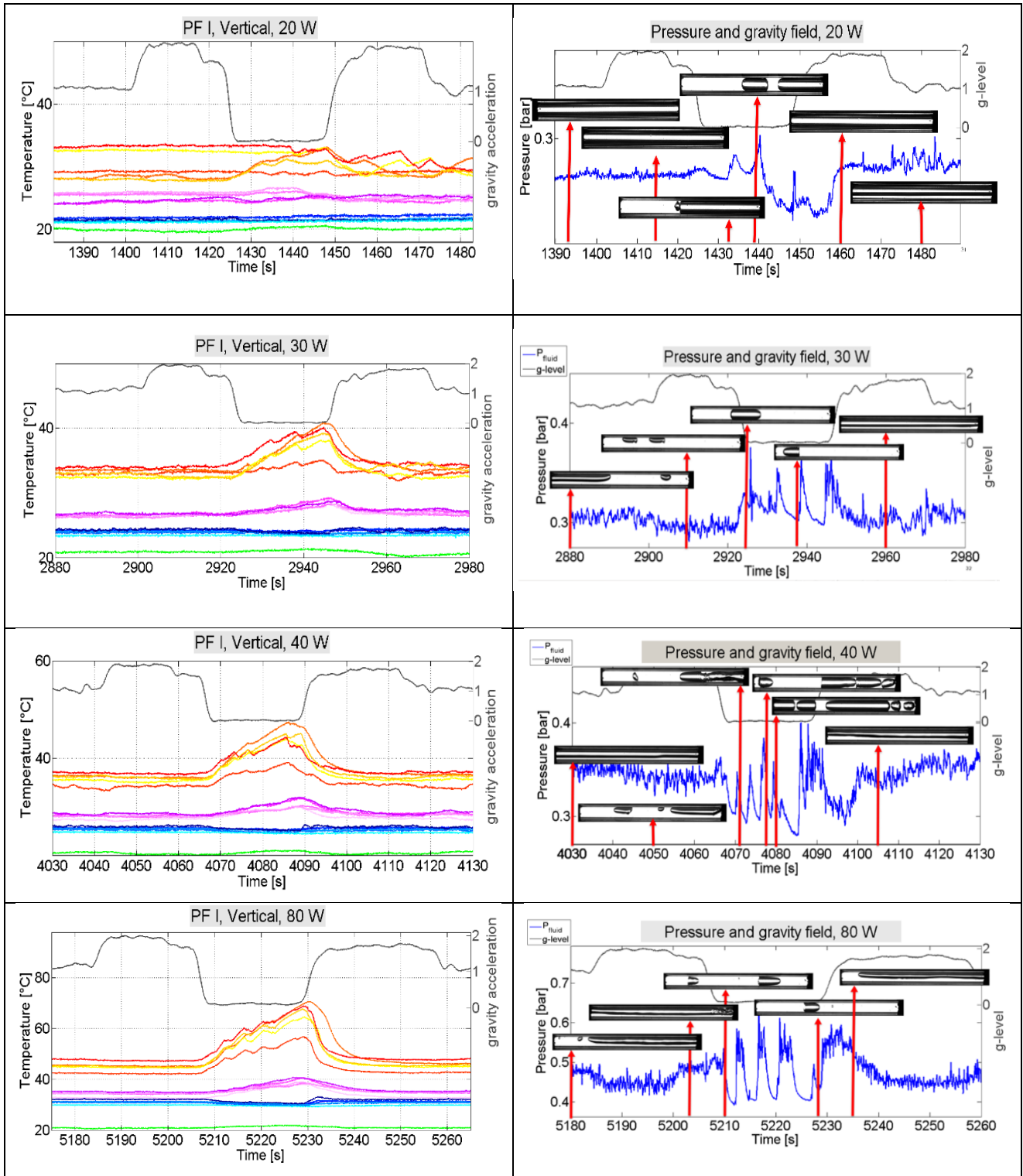
Flight test procedure		
Parabola N.	PF-I (Vertical)	PF-II (Horizontal)
Parabola 0	10 W	10 W
From 1 to 5	20 W	20 W
From 6 to 10	30 W	30 W
From 11 to 15	40 W	40 W
From 16 to 20	80 W	50 W

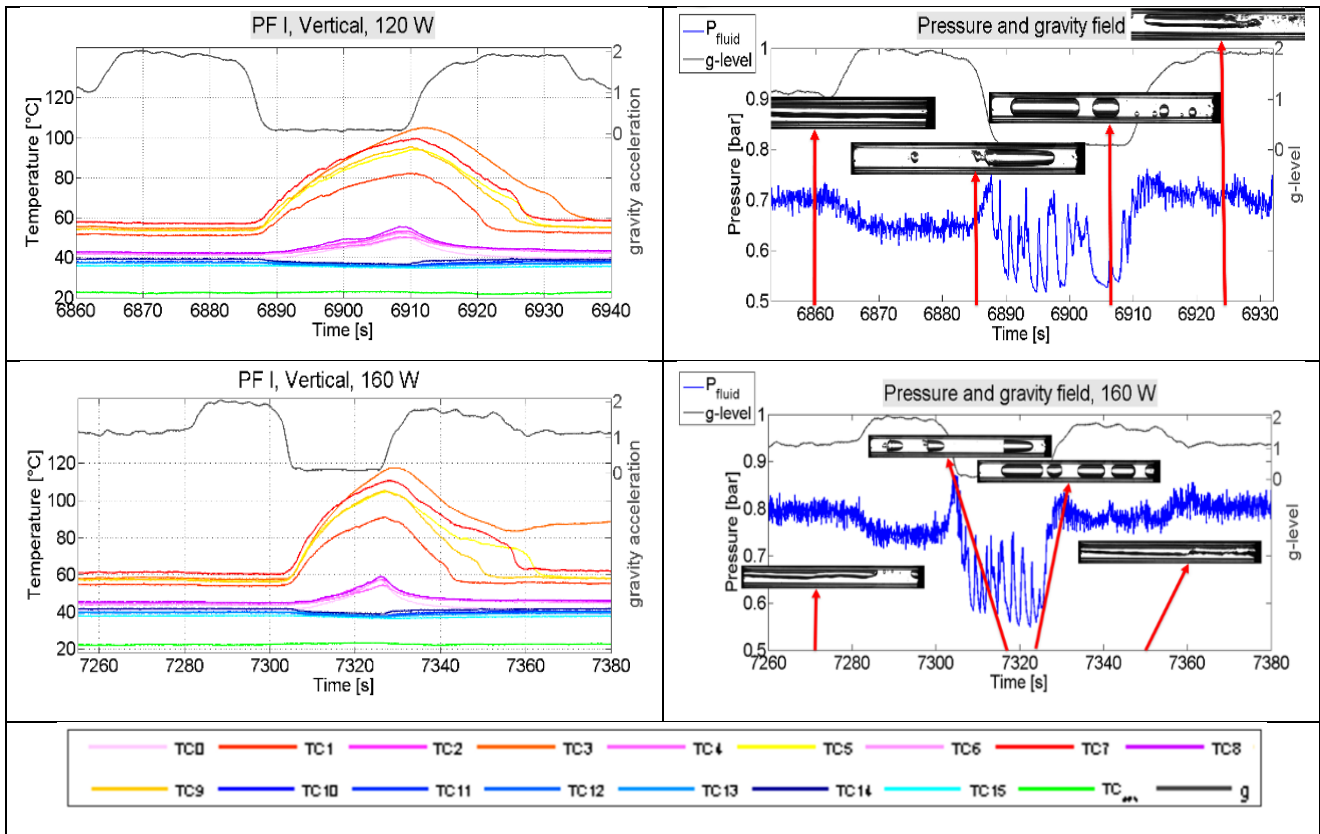
From 21 to 25	120 W	60 W
From 26 to 30	160 W	80 W

256 **3.2.1 Vertical orientation**

257 Focusing on Figure 6, it is possible to recognize the thermal response of the device during the  
 258 gravity field variations. As shown previously, during the ground tests in vertical position, at 10 W  
 259 and 20 W, the heat power is not sufficient to pump the liquid batches in the condenser zone.  
 260 Therefore, during the parabolic flight experiments, the temperatures appear stable in the normal and  
 261 the hyper-gravity conditions, the pressure does not show fluctuations and the transparent section  
 262 remains dry. When the microgravity period starts, a slug/plug flow is observed in the transparent  
 263 condenser section and the temperature values at the evaporator zone decrease rapidly. The liquid  
 264 phase is indeed able to reach more easily the condenser zone when the body force becomes  
 265 negligible during the microgravity period, and the slug/plug flow activation allows the fluid motion  
 266 in the condenser zone, even for the lowest heat power input levels tested. For all the other heat  
 267 power inputs tested, when the device reaches the standard operating conditions as TS, the gravity  
 268 certainly assists the device, giving a net contribution to the fluid momentum. The beginning of  
 269 microgravity, activating the slug/plug flow regime, makes the device to work as a PHP, increasing  
 270 the temperatures at the evaporator zone and decreasing the thermal efficiency. Interestingly, the  
 271 fluid motion does not stop completely in microgravity: the temperatures do not exhibit an ever-  
 272 increasing trend, but the oscillating slug/plug flow motion, increasing the convection, tends to  
 273 stabilize the temperatures.

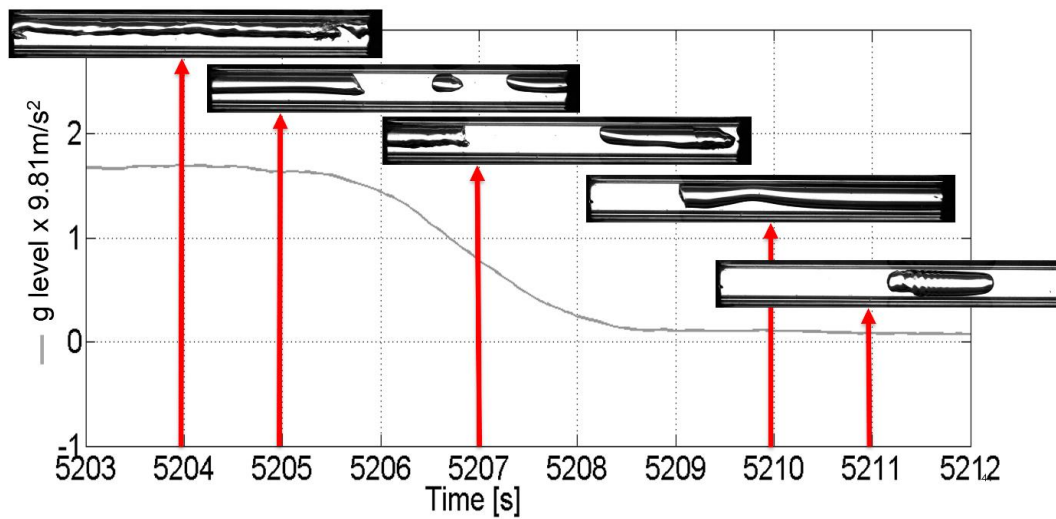






274 **Figure 6: Flight tests in vertical position, first column: temperatures and gravity field; second**  
 275 **column: pressure and gravity field, in conjunction with visual images (red arrows identify the**  
 276 **exact timing of each image).**

277 The temporal evolution in Figure 7, that focuses on the fluid dynamic between the hyper and micro-  
 278 gravity transition, shows that during microgravity, the buoyancy forces become negligible and the  
 279 surface tension of the liquid phase tends indeed to create liquid/vapor interfaces perpendicular to the  
 280 flow path (i.e. menisci). Since the vapor phase fills completely the tube section, the flow pattern  
 281 results in an alternation of vapor plugs and liquid slugs, enabling the device to start working as a  
 282 PHP.

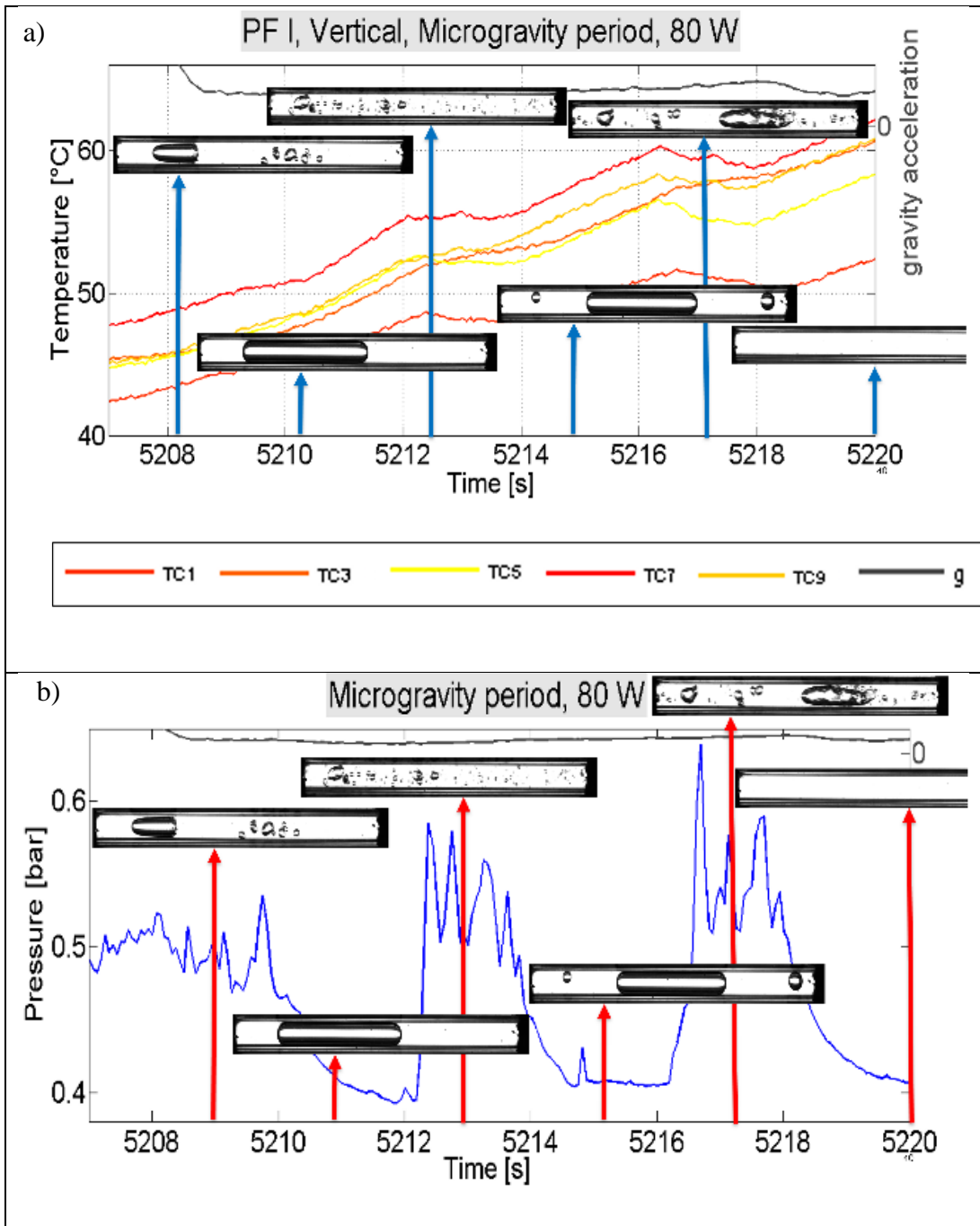


283

284 **Figure 7: Transition from the hyper-gravity period to the micro-gravity period: slug/plug flow**  
 285 **activation.**

286 After the slug/plug flow regime activation, the fluid is no more circulating in a preferential  
 287 direction, but it is characterized by pulsations (typical of a PHP) as shown in Figure 8a, where fluid  
 288 oscillation can be detected both from the pressure transducer readings as well as from the  
 289 corresponding images. When the pressure is nearly constant, the fluid in the condenser zone is not  
 290 moving, and the vapor plugs inside the transparent section of the condenser remain at the same  
 291 position. Such short stop-over periods are followed by vigorous fluid pulsations with a positive  
 292 impact on the heat exchange. Indeed, as soon as the fluid starts to oscillate in the condenser  
 293 transparent section, an abrupt decrease of the evaporator temperatures is also recognizable, as  
 294 shown in Figure 8.

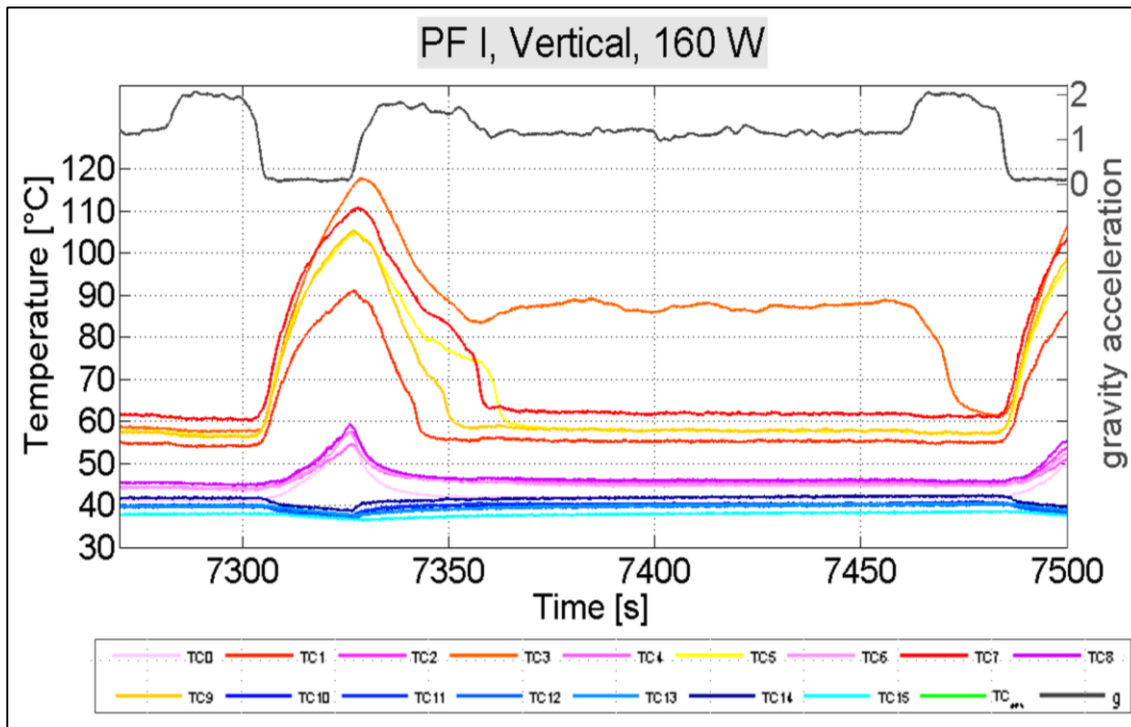




295 **Figure 8: Microgravity period at 80 W; a) temperatures recorded at the evaporator zone; b)**  
 296 **pressure signal and images.**

297 The beneficial effect of gravity, when the device works in TS mode, is recognizable at the highest  
 298 heat power input tested (160 W). In some case for example, after a parabola, the temperature  
 299 recorded by one thermocouple (TC3 in the example of figure 9) sets at approximately 90 °C,  
 300 probably due to a partial dry-out. The next hyper-gravity period is able to eliminate such partial dry-  
 301 out restoring the correct operation until the occurrence of the next microgravity period confirming

302 the results obtained by Mameli et al. [17] on a capillary PHP tested in hypergravity conditions  
 303 aboard ESA Large Diameter Centrifuge.

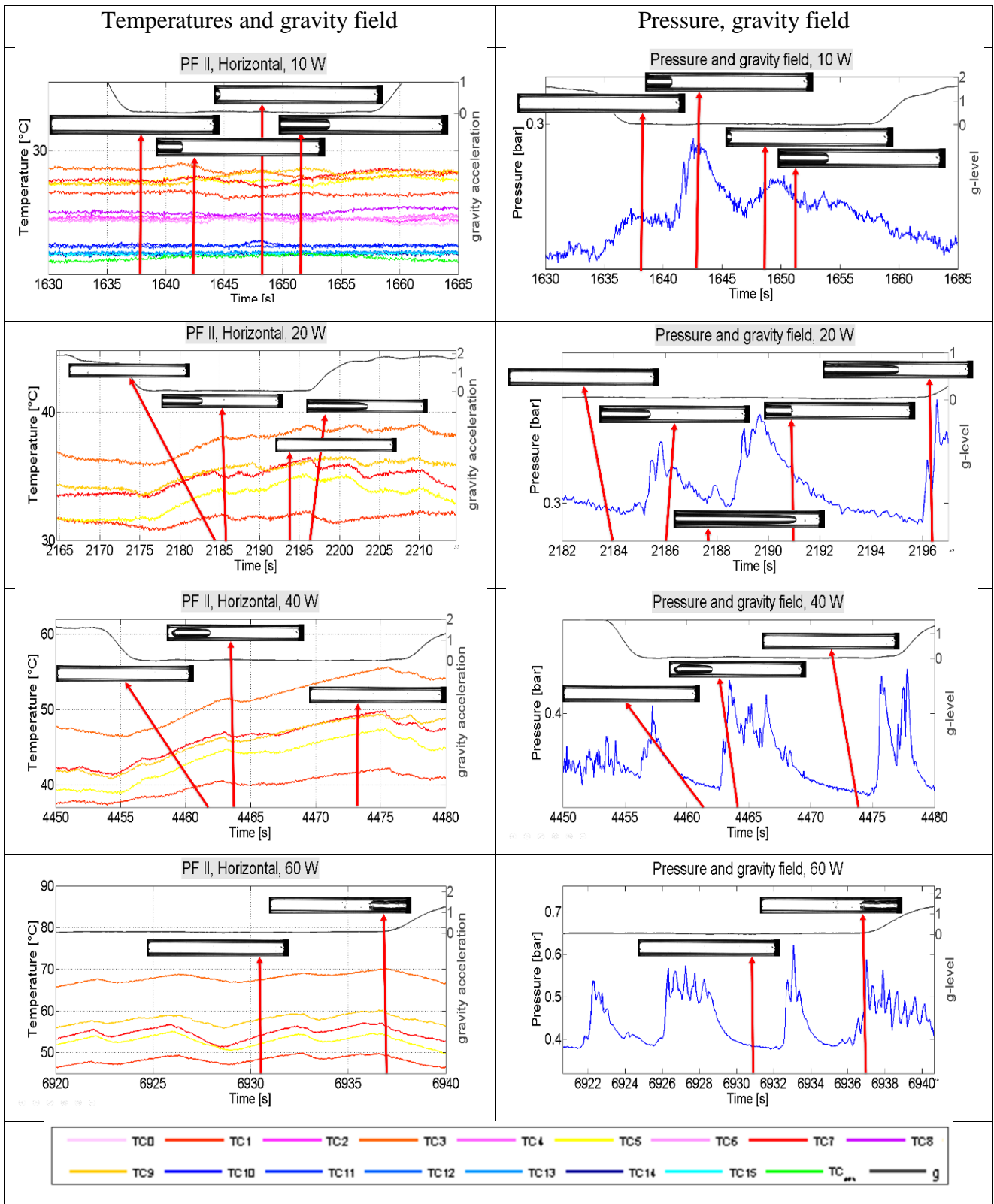


304  
 305 **Figure 9: Hyper-gravity effect on partial dry-out occurred at 160 W.**

306 **3.2.2 Horizontal orientation**

307 During microgravity, the inclination of the device does not play a significant role because of the  
 308 complete absence of the body force: the temperatures and the pressure measurements are similar to  
 309 the microgravity case during the BHM test (PF-I). The vapor plugs, generated during the absence of  
 310 gravity field, are similar to a piston that pumps the liquid columns through the condenser, due to  
 311 their expansion in the evaporator section. This kind of fluid motion is of course beneficial for the  
 312 thermal performance of the device: as soon as the slug/plug flow is activated, the evaporator  
 313 temperatures start to oscillate, as it is depicted in the second column of Figure 10. This is however  
 314 not possible in the normal gravity condition, since the liquid phase fills completely the lowest half  
 315 part of the tube, and there is no possibility to pump the flow in the condenser zone (see Figure 4).

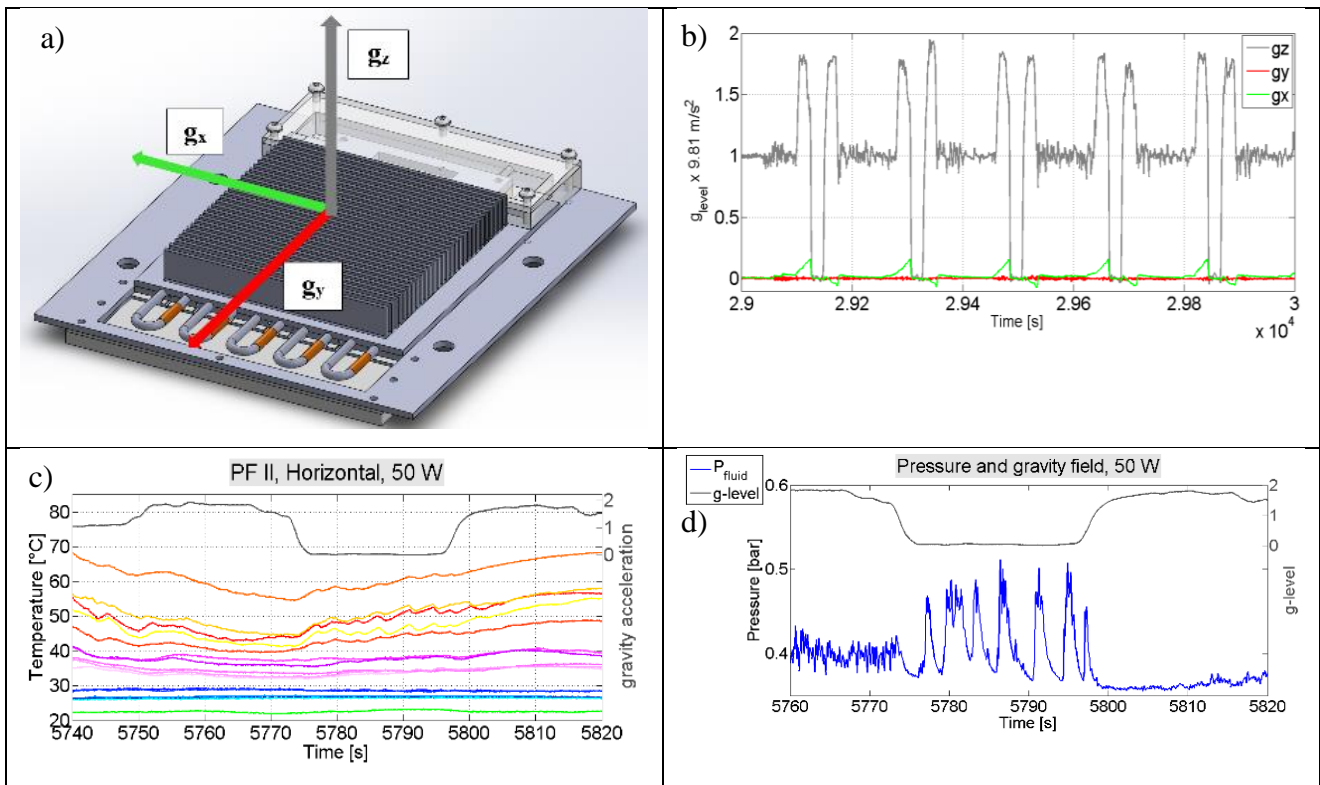
316  
 317  
 318  
 319  
 320  
 321



322 **Figure 10: microgravity period for different heat inputs tested in horizontal orientation; first**  
 323 **column: evaporator temperatures, gravity field and images; second column: pressure, gravity field**  
 324 **and images.**

325 Carefully observing Figure 10, it can be noticed that the fluid motion is often activated during the  
 326 first hypergravity period, causing a sudden decrease in the evaporator temperatures. However, this  
 327 is not occurring during the second hyper-gravity period.

328 This can be explained observing the acceleration components plotted in Figure 11. It is obvious,  
 329 that the proposed activation is not due to the acceleration in the z-direction, but to the “spurious”  
 330 force in the x direction (green line in Figure 11b). During the first hypergravity period due to  $g_x$   
 331 component orientation the generated inertia force causes the fluid to move in the opposite direction,  
 332 improving the beneficial effect due to the thermal asymmetry. However, during the second  
 333 hypergravity period,  $g_x$  is negative inhibiting this preferential fluid motion.



334 **Figure 11:  $g_x$ ,  $g_y$ ,  $g_z$  acceleration components and time evolution during parabolic maneuvers in**  
 335 **horizontal orientation: a) Layout and directions; b)  $g_x$ ,  $g_y$ ,  $g_z$  acceleration over time; c) effect on**  
 336 **temperatures; d) effect on fluid pressure.**

337 This also affects the upcoming microgravity period: evaporator temperatures are decreasing during  
 338 the first hypergravity period (Figure 11c) since the fluid is already moving inside the device as  
 339 witnessed by the fluid oscillations recorded by the pressure transducer (Figure 11d). However, it  
 340 should be mentioned that during micro-gravity all the gravity vector components are close to zero,  
 341 therefore, the fluid motion is mainly due to the slug/plug motion. Summarizing, the parabolic flight  
 342 tests have demonstrated that a transition from the Thermosyphon to the PHP working modes occurs  
 343 during the microgravity periods.

344 **4 CONCLUSIONS**

345 A novel concept of hybrid Thermosyphon/Pulsating Heat Pipe with a diameter bigger than the static  
346 threshold level on ground and around the dynamic threshold level in microgravity conditions (I.D.  
347 of 3 mm filled with FC-72) is tested both on ground and in hyper/micro gravity conditions during  
348 the 61<sup>st</sup> ESA Parabolic Flight Campaign. According to the authors' best knowledge, this is the first  
349 attempt in literature that such a hybrid device is tested. The device is made with an aluminum tube,  
350 equipped with 16 thermocouples (10 at the evaporator zone, 6 in the condenser zone) and with a  
351 pressure transducer in the condenser zone. Moreover, a glass tube (50 mm of axial length) closes  
352 the loop in the condenser zone, allowing also fluid dynamic visualization during gravity field  
353 variations. The temporal trend of the wall temperature, the local fluid pressure in the condenser  
354 zone together with images recorded at 450 fps in the transparent section of the condenser zone,  
355 indicate that the device performance is strongly affected by the variation of the gravity field. In  
356 particular, the following salient points are raised:

- 357 - The device on ground works as a Closed Loop Two Phase Thermosyphon, where the fluid  
358 circulation is activated at high heat input levels thanks to the asymmetric location of the  
359 heating sections reaching an equivalent thermal resistance of 0.1 K/W with heat fluxes up to 17  
360 W/cm<sup>2</sup>.
- 361 - The ground test in horizontal orientation points out that the device works as a pure conductive  
362 medium. No fluid motion is recognized, remarking the importance of a gravity head between  
363 the evaporator one and the condenser zone during the TS mode.
- 364 - The parabolic flight tests reveal that the device operates in a complete different way when the  
365 microgravity is reached: the images recorded in the condenser zone, together with the pressure  
366 signal shows a transition from the Thermosyphon mode to the PHP working mode.
- 367 - The flight test in vertical position points out a start-up also at the lowest heat power input levels  
368 in microgravity. The vapor plugs, expanding in the evaporator zone, permits to the adjacent  
369 liquid column to reach the condenser zone, promoting the heat exchange also at 10 W and 20.
- 370 - During microgravity, a slug/plug pulsating flow is observed also when the PHP is in the  
371 horizontal position.
- 372 - In some cases the hyper-gravity period is able to eliminate partial dry-outs restoring the correct  
373 operation until the occurrence of the next microgravity period.

374

375

376 **ACKNOWLEDGEMENTS**

377 The present work has been carried out in the framework of the Italian Space Agency (ASI) project  
378 ESA\_AO-2009 entitled “Innovative two-phase thermal control for the International Space Station”.  
379 The authors would like to thank the NOVESPACE team in Bordeaux as well as to Dr. Vladimir  
380 Pletser for their support and encouragement during the parabolic flight campaign. The authors  
381 would like to thank Dr. Olivier Minster and Dr. Balazs Toth for their interest and support to the  
382 PHP activities and for the fruitful discussions. Also we acknowledge Ing. Paolo Emilio Battaglia of  
383 the Italian Space Agency for his administrative support. Finally we thank all the members of the  
384 Pulsating Heat Pipe International Scientific Team, led by Prof. Marco Marengo, for their  
385 contribution in pushing the PHP technology for space applications, with a particular gratitude to  
386 Prof. Sameer Khandekar, Dr. Vadim Nikolayev and Dr. Vincent Ayel.

387

388 **REFERENCES**

- 389 [1] G. Gilmore, *Spacecraft Thermal Control Handbook, Vol. 1 Fundamental Technologies*, The  
390 Aerospace Press, El Segundo California, 2002.
- 391 [2] H. Akachi, Structure of a heat pipe. US Patent 4,921,041. (1990).
- 392 [3] M. Mameli, M. Marengo, S. Khandekar, Local Heat Transfer Measurement and Thermo-Fluid  
393 Characterization of a Pulsating Heat Pipe, *J. of Thermal Sci.*,75 (2014) 140-152.
- 394 [4] H. Yang, S. Khandekar, M. Groll, Operational limit of closed loop pulsating heat pipes. *App.*  
395 *Thermal Eng.* 28(1) (2008) 49–59.
- 396 [5] Baldassari C., Marengo M., Flow Boiling in Microchannels and Microgravity Progress in Energy  
397 and Combustion Science, 39(1) (2013) 1–36.
- 398 [6] J. Qu, H. Wu, P. Cheng, Start-up, heat transfer and flow characteristics of silicon-based micro  
399 pulsating heat pipes, *Int. J. of Heat and Mass Transfer* 55 (2012) 6109–6120.
- 400 [7] M. Mameli M., V. Manno, S. Filippeschi, M. Marengo, Thermal instability of a Closed Loop  
401 Pulsating Heat Pipe: Combined effect of orientation and filling ratio, *Exp. Thermal and Fluid*  
402 *Science* 59 (2014) 222–229.
- 403 [8] S.M. Thompson, P. Cheng, H. Ma, An Experimental Investigation of a Three-Dimensional  
404 Flat-Plate Oscillating Heat Pipe with Staggered Microchannels, *Int. J. of Heat and Mass*  
405 *Transfer*, 54 (2011) 3951–3959.
- 406 [9] Y. Maydanik, V.I. Dmitrin, V.G. Pastukhov, Compact cooler for electronics on the basis of a  
407 pulsating heat pipe, *App. Thermal Engineering*, 29 (2009) 3511–3517.
- 408 [10] J. Gu, M. Kawaji, R. Futamata, Effects of gravity on the performance of pulsating heat pipes. *J.*  
409 *Thermophys. Heat Transf.* 18(3) (2004) 370–378.
- 410 [11] J. Gu, M. Kawaji, R. Futamata, Microgravity performance of micro pulsating heat pipe.  
411 *Microgravity Sci. Technol.* 16 (2005) 181–185.
- 412 [12] K.V. Paiva, M.B.H. Mantelli, L.K. Slongo; Experimental Tests of Wire Mini Heat Pipe under  
413 Microgravity Conditions Aboard Suborbital Rockets, 9th IHPS, Malaysia, Nov. 2008.

414 [13]M. Mameli, L. Araneo, S. Filippeschi, L. Marelli,R. .Testa, M. Marengo, Thermal Response Of  
415 A Closed Loop Pulsating Heat Pipe Under A Variable Gravity Force, Int. J. of Thermal  
416 Sciences, 80 (2014) 11-22, DOI 10.1016/j.ijthermalsci.2014.01.023.

417 [14]C.D. Henry, J. Kim, B. Chamberlain, Heater size and heater aspect ratio effects on sub-cooled  
418 Pool boiling heat transfer in low-g, 3rd International Symposium on Two-Phase Flow  
419 Modeling and Experimentation Pisa, 22-24 September 2004.

420 [15]A. Franco, S. Filippeschi, Closed Loop Two Phase Thermosyphon of Small Dimensions: a  
421 Review of the Experimental Results, Microgravity Sci. Technol. 24 (2012) 165-179, DOI  
422 10.1007/s12217-011-9281-6.

423 [16]Novespace A300 Zero-G Rules and Guidelines, RG-2009-2, April, 7th 2009, NOVESPACE  
424 15, rue des Halles 75001 Paris – France.

425 [17] M. Mameli, M. Manzoni, S. Filippeschi, L. Araneo, M. Marengo. Experimental  
426 Investigation on a Closed Loop Pulsating Heat Pipe in Hyper-Gravity Conditions. 15th  
427 International Heat Transfer Conference, Kyoto 10-15 August, 2014.

428  
429  
430  
431  
432  
433  
434  
435  
436  
437  
438  
439  
440  
441  
442  
443  
444  
445  
446  
447  
448  
449  
450  
451  
452  
453  
454  
455  
456

457 **List of figures captions**

458

459 Figure 1: Dynamic threshold diameters for FC-72 for different fluid temperatures evaluated at an  
460 average bulk velocity of the fluid equal to 0.1 m/s and a microgravity level of 0.01 m/s<sup>2</sup>.

461

462 Figure2: a) thermocouples and heaters location along the PHP tube; b) the test cell with all its  
463 components.

464

465 Figure 3: a) air fan system mounted above the heat sink; b) milled heat sink.

466

467 Figure 4: Temperature temporal evolutions, pressure temporal evolutions and equivalent thermal  
468 resistance during thermal characterization on ground, first column: vertical operation, second  
469 column: horizontal operation.

470

471 Figure 5: Fluid net circulation during the vertical tests: a) fluid direction; b) flow visualization  
472 (100 fps); c) temperatures at the edges of the glass tube.

473

474 Figure 6: Flight tests in vertical position, first column: temperatures and gravity field; second  
475 column: pressure and gravity field, in conjunction with visual images (red arrows identify the  
476 exact timing of each image).

477

478 Figure 7: Transition from the hyper-gravity period to the micro-gravity period: slug/plug flow  
479 activation.

480

481 Figure 8: Microgravity period at 80 W; a) temperatures recorded at the evaporator zone; b)  
482 pressure signal and images.

483

484 Figure 9: Hyper-gravity effect on partial dry-out occurred at 160 W.

485 Figure 10: microgravity period for different heat inputs tested in horizontal orientation; first  
486 column: evaporator temperatures, gravity field and images; second column: pressure, gravity field  
487 and images.

488

489 Figure 11:  $g_x$ ,  $g_y$ ,  $g_z$  acceleration components and time evolution during parabolic maneuvers in  
490 horizontal orientation: a) Layout and directions; b)  $g_x$ ,  $g_y$ ,  $g_z$  acceleration over time; c) effect on  
491 temperatures; d) effect on fluid pressure.

492

493

494 **List of tables captions**

495

496 Table 1: Confinement diameters for FC-72 at 20°C accordingly to static and dynamic criteria.

497

498 Table 2. Heat power input levels set up for ground tests.

499



500 Table 3. Heat power inputs during flight days.  
501